Modeling the Ultrasonic Cavitation-Enhanced Removal of Nitrogen Oxide in a Bubble Column Reactor

Yusuf G. Adewuyi and Nymul E. Khan
Dept. of Chemical and Bioengineering, North Carolina A&T State University, Greensboro, NC 27411

DOI 10.1002/aic.12751
Published online September 8, 2011 in Wiley Online Library (wileyonlinelibrary.com).

A model study of the sonochemical removal of nitric oxide (NO) in a bubble column reactor is presented. The detailed model is developed to investigate the actual cavitation phenomena taking place during the absorption of NO. The expansion and subsequent collapse of cavitation bubble according to the theory of cavity collapse—initially developed by Lord Rayleigh and then improved on by coupling the energy balance equation of the bubble and the chemical reactions taking place inside the cavity to calculate the composition of different species formed during the collapse—are modeled. The model takes into consideration (1) cavitation bubble dynamics, (2) generation and transfer of oxidizing species from bubble collapse through reaction kinetics, (3) transfer of NO from gas to liquid, and (4) chemical reactions of oxidizing species with dissolved NO. The results of the simulations surprisingly indicate that the chemistry induced by ultrasonic cavitation cannot explain the absorption of NO beyond about 30% of the inlet concentration if the mass transfer is assumed to be the same as that in the bubble column without ultrasound. When experimental values of mass-transfer coefficients, calculated in the studies by other researchers (which are in the range of about five times the physical mass-transfer coefficient in a bubble column), are used, absorption up to 80% are calculated in the simulations consistent with experimental results obtained from the sonochemical bubble column reactor. The present model provides a framework on which more robust and rigorous models can be developed for the complex gas-liquid sonochemical systems and reactors. © 2011 American Institute of Chemical Engineers *AIChE J,* 58: 2397–2411, 2012

Keywords: bubble column reactor, ultrasonic cavitation, modeling, nitric oxide, simulation

Introduction

NO_x (NO and NO_2) and SO_2—mainly generated from combustion of fossil fuel in power plants and automobiles—have severe detrimental effects on plants, animals, and humans. Numerous environmental and health effects such as acid rain, formation of ground-level ozone, eutrophication, respiratory, and heart diseases in humans are caused by NO_x. Although emissions of NO_2 and SO_2 can be controlled easily by scrubbing, nitric oxide (NO) is not easily removed by aqueous scrubbing due to its very low solubility in such solutions. Ultrasound has been known to enhance the rate of many chemical reactions. Not many studies in the field of ultrasound have focused on gas absorption, especially simultaneous mass transfer with chemical reaction in the presence of ultrasound. The few that have are mostly mass-transfer studies.[1–4] There has been no study in which the gas being absorbed is the primary species that is being removed.

In our previous studies, we demonstrated the absorption of NO (50–1040 ppm) into water and the mechanisms of the simultaneous oxidation to nitrite and nitrate induced by ultrasonic irradiation at a fixed frequency of 20 kHz using a sonochemical bubble column reactor in the absence and presence of SO_2 (52–4930 ppm) at room-temperature (23 $\pm$ 2°C). We also evaluated the effects of ultrasound intensity, presence of NaCl (as an additive), chemical oxidant, and composition of flue gas on the overall NO_x removal.[5,6] The percent fractional conversions of NO were found to range from 60 to 85% while complete removal of SO_2 was observed for all the studied inlet gas concentrations. In addition, the presence of low to moderate concentrations of SO_2 in the inlet gas stream was found to enhance the percent overall NO removal. Also, increasing the ultrasonic intensity was observed to improve the percent overall NO removal. The presence of low concentration of NaCl (0.01 M) enhanced significantly the percent fractional removal of NO with inlet gas concentration of 1040 ppm. The presence of about 2520 ppm SO_2 in combination with 0.01 M NaCl further enhanced NO removal. Combinative effect of sonication and chemical oxidation using 0.005–0.05 M peroxomonosulfate (HSO_5^-) or oxone was also studied. It was demonstrated that lower concentrations of HSO_5^- (0.005 M) enhanced NO removal efficiency.

Sonochemical techniques use ultrasound to produce an oxidative environment via acoustic cavitation due to the formation and subsequent collapse of microbubbles from acoustical wave-induced compression/rarefaction. Ultrasound creates alternating compression and rarefaction pressure fields in a liquid. This causes tiny gas bubbles trapped in the liquid or in the crevices of surfaces to expand and then violently

Correspondence concerning this article should be addressed to Y. G. Adewuyi at adewuyi@ncat.edu.

collapse. During the expansion phase, water evaporates into the bubble and condenses during the collapse.[7] However, as the collapse is extremely fast and almost adiabatic in nature, most of the vapor trapped inside the bubble cannot escape and is disintegrated due to the very high-temperature reached inside the bubble (≈3000–5000 K)[8] to form reactive species such as hydroxyl (·OH), hydroperoxyl ($\cdot HO_2$) radicals or oxygen (O) and hydrogen (H)[7,9] atoms and hydrogen peroxide (H_2O_2).[10] These species diffuse out of the bubble into a thin interfacial layer where they either recombine or react with compounds present in the liquid.

Majority of the studies for the application of sonochemistry are in the field of wastewater treatment. The mechanisms related to the reaction enhancement by cavitation have been elucidated in many studies done on the sonochemical degradation of hazardous organic compounds found in wastewater.[7] In general, three different mechanisms have been proposed to explain the degradation of organic pollutants in wastewater.[7,11] The first is the pyrolysis in the cavitation bubble interior. Within the center of the bubble, harsh conditions generated on bubble collapse cause bond breakage and/or the dissociation of water and other vapors and gases, leading to the formation of free radicals or formation of excited states. Solvent and/or volatile solutes suffer homolytic bond breakage to produce reactive species. The second mechanism is the hydroxylation of the species in the interfacial region by the ·OH radicals generated in the bubble. The H atom does not penetrate very far outside the bubble[12] and, therefore, the ·OH radical is the more prominent species and it is also one with the most oxidative potential of any species in sonochemical systems. The third possible mechanism, proposed by Hoffman and coworkers,[13] is the formation of super-critical water in a small shell around the bubble which promotes the reactions. Other earlier studies have also considered the degradation of gases such as ozone, nitrous oxide, acetylene, and hydrogen sulfide in aqueous solutions and discussed their removal mechanisms and oxidation products.[14–17] The primary mechanism for the decomposition of gases by ultrasound appears to be pyrolysis in the cavitation bubbles with hydroxylation in the interfacial sheath providing secondary pathways. However, in their study using acetylene, Hart et al.[16] found that the dominant mechanism shifts between that of pyrolysis in the bubble core and that of hydroxylation by ·OH radicals at the interface. They concluded that the lower concentration favors reaction pathways in the interfacial zone. Kotronarou and Hoffmann[17] proposed a model for the aqueous phase oxidation of H_2S by ultrasound. A liquid-phase reaction mechanism involving ·OH radicals generated by cavitational collapse was used in their model. By fitting their model results with experimental data, they estimated the uniform release of ·OH radicals into the bulk solution to be of the order of 3.5 μM/min and a steady-state concentration $\leq$0.1 μM.

In view of these studies, it is assumed that NO is oxidized mainly through reaction in the bubble–liquid interface and in the bulk solution with the ·OH radicals (the main oxidant) generated from the bubble interior. In this article, we report the development of a mathematical model for such a system to predict the amount of oxidant in the liquid phase and elucidate the different mechanisms involved. The model relates the bubble dynamics phenomena with the reaction in liquid phase and the simultaneous transfer of mass from the gas to the liquid phase to predict the rate of NO absorption in presence of ultrasound. This comprehensive model takes into consideration (1) cavitation bubble dynamics, (2) generation and transport of oxidizing species from bubble collapse through reaction kinetics, (3) transfer of NO from gas to liquid, and (4) chemical reactions of oxidizing species with dissolved NO. We have used this sonochemistry model to obtain the rate of formation and transfer of ·OH radicals into the liquid, and used the time average of this quantity over one acoustic cycle to determine the average rate of supply of ·OH radical from one cavitation bubble. We have also found the range of total number of bubbles using the average volume of a single bubble and the range of void fractions found experimentally by Tsochatzidis et al.[18] With these two quantities, we have obtained the range of the total rate of supply of ·OH radical into the liquid phase due to ultrasonic cavitation and incorporated this into our liquid-phase kinetic model to predict NO removal.

Experimental Work

The experimental data for this study were collected earlier using an experimental setup (Figure 1) described in details elsewhere.[5,6] The sonochemical bubble column scrubbing system consisted of a jacketed bubble column reactor, a digital sonifier, a flue gas blending system, and an analytical train. The bubble column reactor operated in both semibatch and continuous countercurrent flow. In the semibatch mode of operation, the liquid phase was stationary while the gas phase flowed continuously in the upward direction, whereas in the continuous mode of run, both the liquid and gas phases flowed continuously in countercurrent mode. The ultrasonic system consists of a Branson sonifier (model 450), obtained from Branson with a frequency of 20 kHz and power output of 400 W. The amplitude can be varied to change the power input into the liquid. All the experiments were carried out using a fixed frequency of 20 kHz at or near room-temperature (23 $\pm$ 2°C), with the heat generated from the acoustic excitation removed by the use of a water jacket. The upward flow of the gases through the liquid produces bubbles and promotes the dispersion of the gas into the liquid. At the same time, ultrasonic waves, which promote mixing, are emitted from the sonifier into the solution.

Cavitation model

It is well-known that cavitational activity is concentrated closer to the transducer surface resulting in spatial variation of the cavitational activity. It should also be noted that the local ultrasonic activity and the active cavitational volume in the reactor will also depend on the size and type of reactor, agitation, the presence of solids (size and volume fraction) or flow regimes used in the circulating type of reactor. However, from the current level of knowledge in the area of sonochemical reactors, it is impossible to accurately predict the active and passive zone in the reactor.[19] The complexity of available models such as that of Dähnke and Keil[20] proposed to calculate the three-dimensional pressure fields in a liquid with inhomogeneous distribution of cavitation bubbles limits their application or utility in this study. Therefore, in describing our system, it has been assumed that the microscale phenomena of ultrasonic cavitation takes place uniformly all over the reactor (i.e., the whole liquid phase) generating reactive free radicals, specifically the ·OH radical, the main species which react with the dissolved NO present in the liquid to produce nitrate and nitrite. NO is supplied

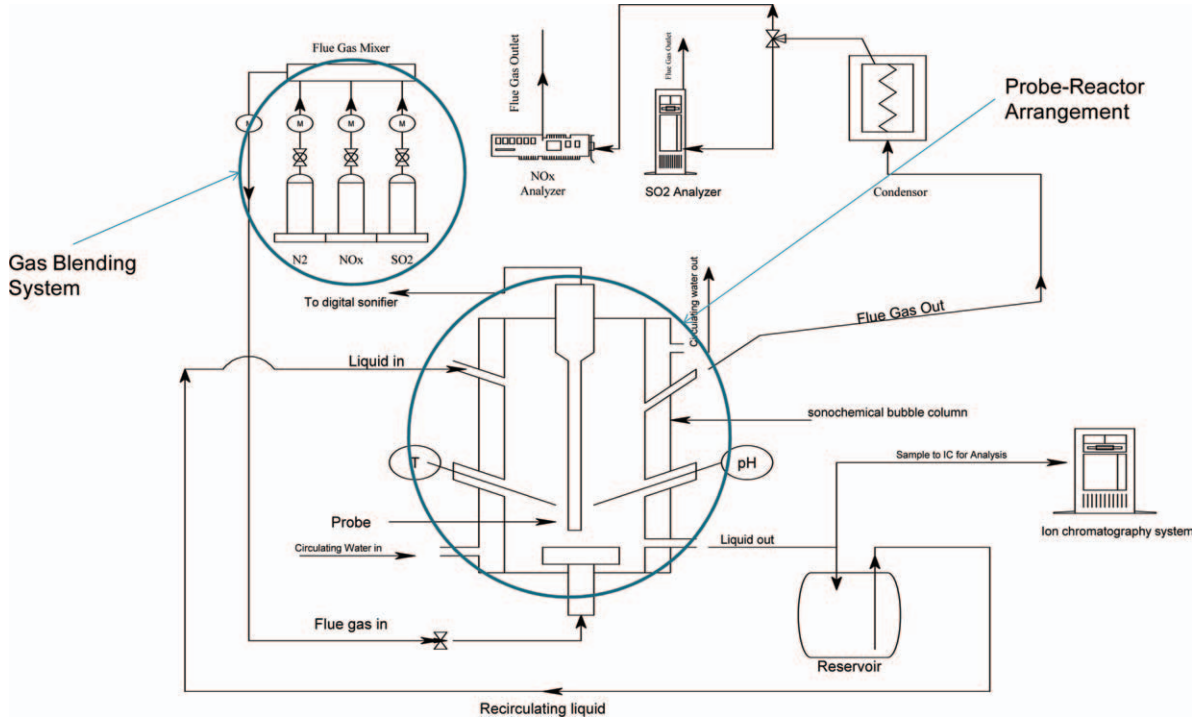

Figure 1. Schematic representation of the sonochemical reactor setup for NO removal.

[Color figure can be viewed in the online issue, which is available at wileyonlinelibrary.com.]

from the gas phase continuously and the concentration of dissolved NO is assumed to be uniform throughout the reactor. This is to be expected since it can be assumed that the liquid phase to be completely back-mixed, which is generally the case in a bubble column, and the bubbles gradually dissolve into the liquid by gas diffusion. In addition, the presence of ultrasound causes greater mixing on top of that. A single bubble sonoluminescence model (SBSL) has been used to describe the cavitation events taking place in the reactor.

SBSL is the phenomenon in which a single oscillating bubble is trapped at the pressure antinode of a standing wave type acoustic generator. The bubble expands to a maximum radius and collapses violently under the influence of the acoustic forcing and emits short pulses of light at a clocklike regularity. It was discovered by Gaitan et al. in 1989.[21] Ideally, the phenomenon taking place in a sonochemical reactor is multibubble sonochemistry. The overall sonochemical oxidation or degradation of a pollutant is a result of collective oscillations and collapse of millions of cavitation bubbles, with strong interaction among them. Although many treatments of multibubble sonochemistry exist in the open literature,[22,23] they are not as developed as SBSL, and may be computationally more intensive than the single bubble analysis. On the other hand, many models exist which predict SBSL processes within order-of-magnitude accuracy.[24–26] Multibubble sonochemistry differs from SBSL in that there is bubble–bubble interaction, which induces shape instability and fragmentation and results in lower-temperatures reached than SBSL.[27,28] In SBSL, where bubble collapse is more spherical and extent of compression greater, sufficient temperatures (even higher than multibubble sonoluminescence, MBSL) are reached.[29] Therefore, the same sonochemical reactions as in MBSL will occur.[30] Although the single bubble analysis does not address entire physics of the sonochemical system, it does provide a qualitative physical insight into the problem as demonstrated by others.[31–33] In view of these attributes, we chose single bubble model for our analysis. The objective of this project was to apply the relatively simpler SBSL to the problem of gas absorption with chemical reaction using ultrasound. The model used in our work is described below.

Bubble Dynamics. The motion of the bubble wall is described by the Keller equation,[34] which is a modification of the well-known Rayleigh–Plesset–Noltingk–Nappiras–Poritsky (RPNNP) equation and takes into account the liquid compressibility

$$\left(1-\frac{\dot{R}}{c_\infty}\right)R\ddot{R}+\frac{3}{2}\dot{R}^2\left(1-\frac{\dot{R}}{3c_\infty}\right) = \frac{1}{\rho_L}\left(1+\frac{\dot{R}}{c_\infty}\right)(P_g-P_s(t)-P_\infty)+\frac{R}{c_\infty\rho_L}\frac{dP_g}{dt} \quad (1)$$

where $\dot{R}$ denotes the time derivative (d/dt), c_∞ is the speed of sound in the liquid, P_s is the time varying pressure field, P_∞ is the hydrostatic pressure, and the pressure at the bubble wall, P_g, is given by

$$P_g(t)=P_i(t)-\frac{1}{R}(2\sigma+4\mu\dot{R}) \quad (2)$$

where σ, μ, and ρ_L denotes the surface tension, viscosity, and density of the liquid, respectively. P_i is the pressure inside the bubble given by van der Waal's equation of state

$$P_i(t)=\frac{R_gT}{\left(\frac{V}{n_t}-b\right)}-\frac{n_t^2a}{V^2} \quad (3)$$

where a and b are van der Waals constants, V is the volume of the bubble, n_t the total number of molecules in the bubble, R_g

is the gas constant, and T is the temperature inside the bubble. When the liquid is irradiated with an acoustic wave of pressure amplitude, P_A and frequency, f, $P_s(t)$ is given by Eq. 4

$$P_S(t) = -P_A \sin(2\pi ft) \tag{4}$$

The RPNNP equation exists in other various forms in the open literature.[34–39] We chose the Keller form of the RPNNP equation for this study based on the work of Prosperetti and Lezzi, which tested this form against other equations of the family and found this form to be most accurate for test cases considered.[34]

Mass Transport. The current models for SBSL include the diffusion of gas and water vapor into the bubble. In single bubble sonoluminescence with air as the saturating gas, the "argon rectification hypothesis" states that the non-noble gases in an air bubble undergo chemical reactions into soluble products, leaving only argon with soluble species ·OH, H_2O_2, or NH_3. The rates at which the soluble species are expelled from the bubble are assumed to be proportional to the rate at which they strike the bubble interface. A diffusive equilibrium is finally reached when the amount of gas diffusing into the bubble in one acoustic cycle has the polyatomic species (e.g., N_2) lost to chemical reactions by completely reacting with water vapor in the subsequent collapse to soluble species such as NO_x and HNO which are taken up by the water outside the bubble, causing the bubble to attain a stable size that does not grow or shrink over the course of time and whose entire content is inert gas (i.e., nearly pure argon, the main inert component in air).[30] Thus, a sonoluminescing air bubble rectifies argon, the only substance inside the bubble that does not dissociate, which is contained in air with a concentration of 1%. The theory provides quantitative explanations for many aspects of SBSL. However, this phenomenon becomes significant only over long period of time. In our case, we assume that transient cavitation, in which the bubble oscillates over one or few acoustic cycles before breaking up into smaller bubble, is the dominating process, as is the case at high amplitude ultrasound. Hence, in our mass-transfer model, we neglect rectified diffusion (i.e., the diffusion or net inflow of gases across the bubble wall) as the time scale for the diffusion gases (which is of the order of few milliseconds) is much higher than the time scale for the radial motion of bubble (which is of the order of microseconds).[40] As an example, for the time scale of diffusion of gas ($\approx R_0^2/D$) where D is the diffusion coefficient, and representative values such as $R_0 \approx 10$ μm and $D \approx 10^{-9}$ m^2/s, the value is 0.1 s which is far higher than the time scale of the bubble dynamics (or ultrasound wave): 50 μs for 20 kHz wave.[41]

On the other hand, the transport of water vapor across the bubble boundary is very important, as it is the main reactant for the production of free radicals and the prime limiter of the temperature reached in the bubble. Two mechanisms have been discussed in literature on water vapor transport into the bubble—the nonequilibrium phase change at the wall and the diffusion to and from the interior of the bubble. Nonequilibrium phase change occurs when the vapor and condensed phase are not in equilibrium. Yasui assumed that the transport of mass through the boundary layer was condensation limited rather than diffusion limited (mass transfer was not explicitly modeled, and, thus, assumed instantaneous).[42,43] Yasui et al.[24] also carried out simulations using different models, including the diffusion-limited model and the phase change limited model and compared them with experimental data from Didenko and Suslick.[44] They found that there is little difference between the diffusion-limited model and the phase change model. We have used the latter as the mechanism controlling the water vapor transport.

Water vapor constantly changes phase at the bubble wall due to the intense volume oscillations of the bubble. The process is driven by the nonequilibrium between the partial pressure of water vapor inside the bubble and the saturation pressure at the interface. The phase changes across a liquid-gas interface are usually observed to take place in pressure, temperature, and mass concentration fields with steep gradients. This requires treatment from the standpoint of kinetic theory, due to molecular nonequilibrium effects in such systems. Evaporation and condensation take place at a finite rate. If this rate is not high enough to keep up with the reducing rate of the volume of the cavity, the vapor in the cavity will behave like a noncondensable gas. This is the so-called nonequilibrium effect. It should also be noted that heat transfer to an interface undergoing a phase change is used not only to change phase but also to impart kinetic energy of the fluid. The net rate of evaporation ($\dot{m}$) is calculated from the kinetic theory of gases (Eq. 5) and the flux of water vapor due to the nonequilibrium phase change is given by the Hertz–Knudsen–Langmuir formula (Eq. 6).[35,45–47]

$$\dot{m} = \dot{m}_{eva} - \dot{m}_{con} \tag{5}$$

$$\dot{m}_{eva} = \frac{\alpha}{\sqrt{2\pi R_v}} \left(\frac{p^*(T_L)}{\sqrt{T_L}} \right) \tag{6}$$

$$\dot{m}_{con} = \frac{\alpha}{\sqrt{2\pi R_v}} \left(\frac{\Gamma p_v}{\sqrt{T}} \right) \tag{7}$$

where α is the mass accommodation coefficient for evaporation or condensation. It is a rate parameter corresponding to the mass transfer at the interface and indicates the portion of vapor molecules striking the liquid surface (i.e., phase interface) that is absorbed (literature[48] suggests a value between 0.17 and 0.32 so we used a value on the lower end, i.e., 0.17 assuming it is constant); p^* is the saturated or equilibrium vapor pressure and p_v is the partial pressure of water in the bubble; R_v is the gas constant of water vapor; and T and T_L are the temperature of the vapor and liquid at the phase interface, respectively. The correction factor (Γ), is given by Eq. 8

$$\Gamma = \exp - (\Omega^2) - \Omega\sqrt{\pi} \left(1 - \frac{2}{\sqrt{\pi}} \int_0^{\Omega} \exp(-x^2) dx \right) \tag{8}$$

where Ω is

$$\Omega = \frac{\dot{m}}{p_v} \left(\frac{R_v T}{2} \right)^{\frac{1}{2}} \tag{9}$$

Using this, the variation of water molecules in the bubble due to the nonequilibrium phase change is calculated as[49–51]

$$\left(\frac{dn_w}{dt} \right)_d = 4\pi R^2 \frac{10^3 N_A}{M_{H_2O}} \dot{m} \tag{10}$$

where n_w is the number of molecules of water in the bubble, M_{H_2O} is the molar mass of water, and N_A is the Avogadro's

constant. Therefore, the total rate of change of water vapor (molecules per second) in the bubble is given by the following expression

$$\frac{dn_w}{dt} = 4\pi R^2 \frac{10^3 N_A}{M_{H_2O}} \dot{m} + \frac{4}{3}\pi R^3 \sum_j \alpha_{H_2O,j} r_j \tag{11}$$

The second term represents the consumption by chemical reaction where $\alpha_{H_2O,j}$ is the stoichiometric coefficient of water in jth reaction and r_j is the rate expression of jth reaction. The kinetic term will be explained in a later section.

Energy Balance. The temperature in the bubble is influenced by a number of processes. The heating of the gas due to compression, the energy carried by water molecules when they evaporate or condense at the wall, the conduction of heat to and from the bubble and the chemical reactions all play important roles at different phases of the bubble oscillation to change the temperature of the bubble. The application of the first law of thermodynamics for an open system yields

$$\frac{dU}{dt} = \frac{dQ}{dt} + \frac{dW}{dt} + (h_w + e_{form,w})\left(\frac{dn_w}{dt}\right)_d \tag{12}$$

Here, dU/dt is the change in internal energy, dQ/dt is the heat transfer across the bubble wall, dW/dt is the work done on the bubble, the last term on the right is the energy carried by water vapor transporting across the bubble wall, h_w is the molecular enthalpy of water vapor at the cold bubble wall, and $e_{form,w}$ is the enthalpy of formation of water vapor. The total internal energy (U) is a function of the temperature (which results from acoustic energy supply) and volume of the bubble, and the number of various species in it. We have considered water molecules as the dominant species.

The total energy of the bubble is given by

$$U = \sum_i (e_{th,i} + e_{form,i}) n_i \tag{13}$$

where $e_{th,i}$ denotes the thermal energy and $e_{form,w}$ denotes the enthalpy of formation of species i. Differentiating this with respect to time we get

$$\frac{dU}{dt} = \frac{dT}{dt}\sum_i \frac{\partial e_{th,i}}{\partial T} n_i + \sum_i (e_{th,i} + e_{form,i}) \frac{dn_i}{dt} \tag{14}$$

Combining Eq. 12 with Eq. 14 and taking $\frac{dn_i}{dt} = \left(\frac{dn_w}{dt}\right)_d + \frac{dni}{dt}_c$ we have

$$\frac{dT}{dt}\sum_i \frac{\partial e_{th,i}}{\partial T} n_i = \frac{dQ}{dt} + \frac{dW}{dt} + (h_w - e_{th,w})\frac{dn_w}{dt} + \sum_i e_{form,i}\left(\frac{dn_i}{dt}\right)_c \tag{15}$$

The term $\sum_i e_{form,i}\left(\frac{dn_i}{dt}\right)_c$ is the heat of reaction which is replaced by an equivalent expression $V\sum_i \left(\frac{dn_i}{dt}\right)_c \Delta H_i^f$ where ΔH_i^f is the heat of formation of species i.

Yasui[46] constructed a thermal conduction model considering thermal boundary layers in both gas and liquid and a temperature jump at the interface between gas and liquid phases. They have assumed the temperature gradient to reside in a thin layer at the wall and the temperature in the bubble to be otherwise uniform. The thickness of this boundary layer is assumed to be $n\lambda$ where λ is the mean free path of a gas molecule and n is a constant found to be 7 by fitting experimental data.[46] It is assumed that the temperature in the boundary layer changes linearly. Therefore, the temperature gradient is given by

$$\frac{\partial T}{\partial r}\Big|_{r=R} = \frac{T_B - T}{n\lambda} \tag{16}$$

T_B is the gas temperature at the bubble wall and T is the temperature inside the bubble. The mean free path is calculated by Eq. 17

$$\lambda = \frac{V}{\sqrt{2}\sigma' n_t} \tag{17}$$

where σ' [0.4×10^{-18} (m^2) is assumed] is the collision cross section of a molecule in the bubble and n_t is the total number of molecules.[35] The temperature jump (ΔT) at the interface between gas and liquid follows from the kinetic theory of gases[26,35]

$$T_B = T_L + \Delta T \tag{18}$$

where T_L is the liquid temperature. In general, temperature jump is a property associated with the discontinuity which exists in the temperature distribution of nonuniform gases near a surface or phase boundaries.[51–53] Temperature jump occurs over a distance equal to about one mean free path of the gas (λ). The expression for the temperature jump (ΔT) is

$$\Delta T = -\frac{1}{2kn'}\sqrt{\frac{\pi m}{2kT_B}}\frac{2 - a'\alpha_e}{\alpha_e} K \frac{\partial T}{\partial r}\Big|_{r=R} \tag{19}$$

Thermal conduction models with temperature jump at the bubble wall and absence of temperature gradient in the liquid phase have been used by other investigators and tested well against experimental data.[46,52,53] The rate of heat transfer through the wall is given by Eq. 20

$$\frac{dQ}{dt} = 4\pi R^2 K \frac{\partial T}{\partial r}\Big|_{r=R} \tag{20}$$

where K is the thermal conductivity of the gas. The thermal conductivity depends on temperature and density of the gas and vapor, the dependence is assumed to be linear (i.e., $\kappa(T) = \beta + \alpha T$). For argon, $\beta = 0.009$ W/mK and $\alpha = 3.2 \times 10^{-5}$ W/mK^2, which give a reasonable representation over the range 250–2000 K.[39,42] The work done on the bubble is

$$\frac{dW}{dt} = -P_g \frac{dV}{dt} = -4\pi R^2 P_g \frac{dR}{dt} \tag{21}$$

Using Eqs. 15, 20, and 21, the differential equation for temperature in the bubble interior becomes

$$\frac{dT}{dt}\sum_i \frac{\partial e_{th,i}}{\partial T} n_i = 4\pi R^2 K \frac{\partial T}{\partial r}\Big|_{r=R} + - 4\pi R^2 P_g \frac{dR}{dt} + (h_w - e_{th,w})\frac{dn_w}{dt} + \sum_i \left(\frac{dn_i}{dt}\right)_c \Delta H_i^f \tag{22}$$

Table 1. Chemically Reactive Species $i = 1, \ldots, 7$ Considered in Our Model

i	Species	f_i	$\Theta_{i,1}$	$\Theta_{i,2}$	$\Theta_{i,3}$
1	H_2	5	6325		
2	O_2	5	2273		
3	OH	5	5370		
4	H_2O	6	2295	5255	5400
5	NO	5	2710		
6	NO_2	6	1878	1064	2272
7	N_2	5	3350		
8	Ar	3			

In addition, argon ($i = 8$) is allowed for. Given are the number f_i of the translational + rotational degrees of freedom and the characteristic vibrational temperatures $\Theta_{i,l}$. The molecular enthalpy follows from the number of degrees of freedom as $h_w = \left[\frac{f_i+2}{2}\right] kT_0$. The parameter data have been taken from Ref. 54.

The value of $e_{th,i}$ is given by the expression[54]

$$e_{th,i} = \left(\frac{f_i}{2} kT + \sum_l \frac{k_{\Theta_{i,l}}}{\exp\left(\frac{\Theta_{i,l}}{T}\right) - 1} \right) \tag{23}$$

and f_i and $\Theta_{i,l}$, $l = 1, ..., l_{max}$, denotes the number of translational and rotational degrees of freedom and the characteristic vibrational temperatures of species i, the values are summarized in Table 1.

Chemical Kinetics. There are two general approaches available to calculate the composition of the bubble. One is a thermodynamic approach[31–33,55–57] and other is the kinetic approach.[24,54,58–60] In the former approach, the bubble is assumed to be in thermodynamic equilibrium at the end of a collapse and the composition is found by carrying out a Gibbs' energy minimization. On the other hand, in the second approach, rates of chemical reactions are used to calculate the composition of the bubble with time. Chemical reactions are the source of the free radicals and a significant process that consumes the energy of the bubble.[43,59,61] Use of chemical reaction yields the composition of the bubble at each time interval so the development of the composition profiles with time can be followed. Using this approach also allows us to incorporate the heats of reaction, as previously shown. Also, the thermodynamic approach inherently assumes that the kinetic time scales are much larger than the dynamic time scale. For these reasons, a kinetic approach is taken to calculate the composition of the bubble. A total of 49 reactions involving 19 species have been taken into account.[60] Each of these elementary reactions has a forward and backward rate per unit volume, $r_{f,j}$,$r_{b,j}$, which is described by means of modified Arrhenius laws

$$r_{f,j} = A_{f,j} T^{B_{f,j}} \exp\left(\frac{-c_{f,j}}{T}\right) \Pi_i N_i^{\nu} \tag{24}$$

$$r_{b,j} = A_{b,j} T^{B_{b,j}} \exp\left(-\frac{c_{b,j}}{T}\right) \Pi_i N_i^{\nu_{j,i}} \tag{25}$$

where A_j, B_j, and C_j are rate constants corresponding to jth reaction. The reactions inside an air bubble resulting in the generation of OH radicals and values of these parameters are listed in Table 2. For a bubble containing water vapor and air, chemical reactions taken into account involve N_2, O_2, H_2O, OH, H, O, HO_2, H_2O_2, O_3, N, HNO_2, HNO, HNO_3, NO, NO_2, and N_2O. In general "M" is the third body which plays an important role in the reactions supplying the energy required for dissociation or absorbing the energy released by recombination and is often denoted as the total mass of the gases and vapor inside the bubble.[62,63] Here, as indicated in Table 2, it is the sum of the concentrations of all the species. The overall rate is given by the difference of forward and backward rate

$$r_j = r_{f,j} - r_{b,j} \tag{26}$$

and the chemical rate of change of species i by the sum over all elementary reaction rates with their proper stoichiometric weight $\alpha_{i,j}$

$$\left(\frac{dn_i}{dt}\right)_c = V \times \sum_j \alpha_{i,j} r_j \tag{27}$$

where V is the bubble volume.

Extrapolation of SBSL model to a sonochemical reactor

The great advantage of using SBSL in this study is that, in contrast to MBSL, the mechanics of SBSL is well understood and characterized. As noted by Brenner et al., it thus seems possible that one will be able to use SBSL to carefully study chemical reactions under exotic conditions of high-temperatures and extreme densities.[43] The above model for a single bubble furnishes information about the amount of ·OH radicals generated at the collapse and the change of bubble volume over one acoustic cycle. Using these two quantities, we can determine the range of the number of cavitation bubbles in a sonochemical reactor and subsequently the rate of generation of the ·OH radical. The mass transfer of NO from gas bubbles entering the reactor together with the reaction scheme in the liquid phase (Table 3) is then used to predict the rate of removal of NO.

Yasui et al.[24] have suggested an expression to calculate the rate of dissolution of the different species in the liquid using uptake coefficient (Θ)

$$r_{d,i} = \Theta \sqrt{\frac{kT_B}{2\pi m_i}} \frac{n_i}{V} \times 4\pi R^2 \tag{28}$$

where m_i is the molecular mass of the species. The time-averaged rate of dissolution of ·OH radicals over one acoustic cycle from a single bubble is

$$\langle r_{d,OH}(R_0) \rangle_t = \frac{\int_0^{t_{cycle}} r_{d,OH}(R_0, t) dt}{t_{cycle}} \tag{29}$$

where $\langle\rangle_t$ represents averaged quantity over t. The average volume of a bubble over one acoustic cycle is

$$\langle V(R_0) \rangle_t = \frac{\int_0^{t_{cycle}} V(R_0, t) dt}{t_{cycle}} \tag{30}$$

Some recent studies have characterized velocity and bubble population (size, concentration, or number distribution) of ultrasonic cavitation bubble in sonochemical reactors.[18,66–68] Tsochatzidis et al.[18] have determined the number and velocity distribution of cavitating bubbles in a sonochemical reactor using a sophisticated technique. The reactor geometries and

Table 2. The Important Chemical Reactions Inside an Air Bubble

Chemical Reaction	A_f	B_f	C_f	A_b	B_b	C_b
$H_2O + M \rightarrow OH + H + M$	1.96E+16	−1.62	59,700	2.25E+10	−2	0
$O_2 + M \rightarrow O + O + M$	1.58E+11	−0.5	59,472	6.17E+03	−0.5	0
$H + O_2 \rightarrow O + OH$	1.92E+08	0	8270	7.18E+05	0.36	−342
$H_2O + O \rightarrow OH + OH$	2.21E+03	1.4	8368	2.10E+02	1.4	200
$O + H_2 \rightarrow OH + H$	5.08E−02	2.67	3166	2.64E−02	2.65	2245
$OH + M \rightarrow O + H + M$	4.66E+11	−0.65	51,200	4.72E+06	−1	0
$H_2O + OH \rightarrow H_2O_2 + H$	1.41E+05	0.66	12,320	4.82E+07	0	4000
$HO_2 + OH \rightarrow H_2O_2 + O$	4.62E−03	2.75	9277	9.55E+00	2	2000
$O + O_2 + M \rightarrow O_3 + M$	4.10E+00	0	−1057	2.48E+08	0	11,430
$OH + O_2 \rightarrow O_3 + H$	4.40E+01	1.44	38,600	2.30E+05	0.75	0
$H + O_3 \rightarrow O + HO_2$	9.00E+06	0.5	2010	–	–	–
$O_2 + OH \rightarrow O + HO_2$	3.10E+06	0.26	26,083	1.81E+07	0	−200
$H_2O_2 + M \rightarrow OH + OH + M$	1.20E+11	0	22,900	9.00E−01	0.9	−3050
$N_2 + O_2 \rightarrow O + N_2O$	6.30E+07	0	55,200	1.00E+08	0	14,100
$N_2O + H \rightarrow OH + N_2$	7.60E+07	0	7600	2.50E+06	0	39,000
$NO_2 + M \rightarrow O + NO + M$	1.10E+10	0	33,000	1.10E+03	0	−940
$O_2 + N \rightarrow O + NO$	6.40E+03	1	3150	1.50E+03	1	19,500
$NO_2 + H \rightarrow OH + NO$	3.50E+08	0	740	2.00E+05	0.5	15,500
$NO + HO_2 \rightarrow OH + NO_2$	3.00E+06	0.5	1200	1.00E+05	0.5	6000
$HNO_2 + O \rightarrow OH + NO_2$	6.00E+05	0	2000	–	–	–
$HNO + O \rightarrow OH + NO$	4.90E+05	0.5	1000	–	–	–
$HNO_3 + O \rightarrow OH + NO_3$	6.00E+05	0	4000	–	–	–
$NO_3 + H \rightarrow OH + NO_2$	3.50E+08	0	750	–	–	–
$O + N + M \rightarrow NO + M$	6.40E+04	−0.5	0	4.00E+14	−1.5	75,500
$O + N_2 \rightarrow NO + N$	7.60E+07	0	38,000	1.60E+07	0	0
$O + HNO_2 \rightarrow HNO + O_2$	3.00E+06	0	8000	–	–	–
$O + N_2O \rightarrow HNO + O_2$	1.00E+08	0	14,100	1.30E+06	0	32,100
$O + NO_2 \rightarrow NO + O_2$	1.00E+07	0	300	1.70E+06	0	23,400
$O + NO_2 + M \rightarrow NO_3 + M$	1.10E+07	0	0	2.50E+03	–	–
$O + HNO_3 \rightarrow O_2 + HNO_2$	6.00E+06	0	8000	–	–	–
$OH + N \rightarrow NO + H$	4.50E+07	0	0	1.70E+08	0	24,500
$OH + NO + M \rightarrow HNO_2 + M$	8.00E+03	0	1000	5.10E+11	−1	25,000
$OH + HNO_2 \rightarrow H_2O + NO_2$	1.50E+06	0	28	8.40E+05	0	21,136
$OH + NO_2 + M \rightarrow HNO_3 + M$	5.00E+05	0	0	1.60E+09	0	15,400
$OH + H_2 \rightarrow H + H_2O$	2.18E+02	1.51	1726	1.02E+03	1.51	9370
$OH + HNO \rightarrow NO + H_2O$	3.60E+07	0	0	2.40E+00	0	0
$OH + OH \rightarrow HO_2 + H$	1.08E+05	0.61	18,230	1.69E+08	0	440
$H_2O_2 + H \rightarrow H_2 + HO_2$	4.82E+07	0	4000	1.41E+05	0.66	12,320
$H_2O_2 + OH \rightarrow H_2O + HO_2$	1.00E+07	0	900	2.80E+07	0	16,500
$O_3 + H \rightarrow HO_2 + O$	9.00E+06	0.5	2010	–	–	–
$O_3 + H \rightarrow OH + O_2$	2.30E+05	0.75	0	4.40E+10	1.44	38,600
$HNO + M \rightarrow NO + H + M$	3.00E+10	0	24,500	5.40E+03	0	−300
$H + O_2 + M \rightarrow HO_2 + M$	2.00E+03	0	−500	2.46E+09	0	24,300
$HNO_2 + H \rightarrow H_2 + NO_2$	4.90E+05	0.5	1500	2.40E+07	0	14,500
$N_2 + M \rightarrow N + N + M$	3.70E+15	−1.6	113,200	3.00E+02	0	−500
$NO + NO_3 \rightarrow NO_2 + NO_2$	4.10E+08	0	481	3.90E+05	0	12,000
$H_2 + M \rightarrow H + H + M$	4.58E+13	−1.4	52,500	2.45E+08	−1.78	480
$H_2 + O_2 \rightarrow HO_2 + H$	2.19E+07	0.28	28,390	6.63E+07	0	1070

M is the third body and is given by the sum of the concentrations of all the species. The rate of each reaction is calculated by the formula similar to Eqs. 24 and 25. Subscript "f" denotes the forward reaction and "b" denotes backward reaction. A (frequency factor) is in "m^3/mol s" for a two-body reaction, "m^6/mol^2 s" for a three-body reaction and C_f (activation temperature) is in Kelvin. The reactions and parameters are collected from Refs. 24 and 60.

Table 3. Possible Reactions Occurring in the Aqueous Phase

No.	Reaction	Second-Order Rate Constant (L/(mol s)	Ref.
1	$NO + OH \rightarrow H^+ + NO_2^-$	2×10^{10}	64
2	$OH + OH \rightarrow H_2O_2$	5.5×10^9	64
3	$OH + H_2O_2 \rightarrow O_2^- + H_2O$	2.4×10^7	64
4	$O_2^- + OH \rightarrow OH^- + O_2$	7×10^9	64
5	$OH + OH^- \rightarrow O^- + H_2O$	1.3×10^{10}	64
6	$NO_2^- + OH \rightarrow NO_2 + OH^-$	1×10^{10}	64
7	$NO_2 + OH \rightarrow HNO_3$	1×10^{10}	64
8	$O_2^- + NO \rightarrow ONOO^-$	$4.3 \pm 0.5 \times 10^9$	65
9	$O^- + H_2O \rightarrow OH^- + OH$	1.7×10^6	64
10	$O^- + OH \rightarrow HO_2^-$	$\leq 2 \times 10^{10}$	64
11	$H_2O_2 \leftrightarrow H^+ + HO_2^-$	$pK = 11.65$	17
12	$HNO_2 \leftrightarrow H^+ + NO_2^-$	$pK = 3.15$	17
13	$HO_2 \leftrightarrow H^+ + O_2^-$	$pK = 4.46$	17
14	$HNO_3 \leftrightarrow H^+ + NO_3^-$	$pK = -1.3$	

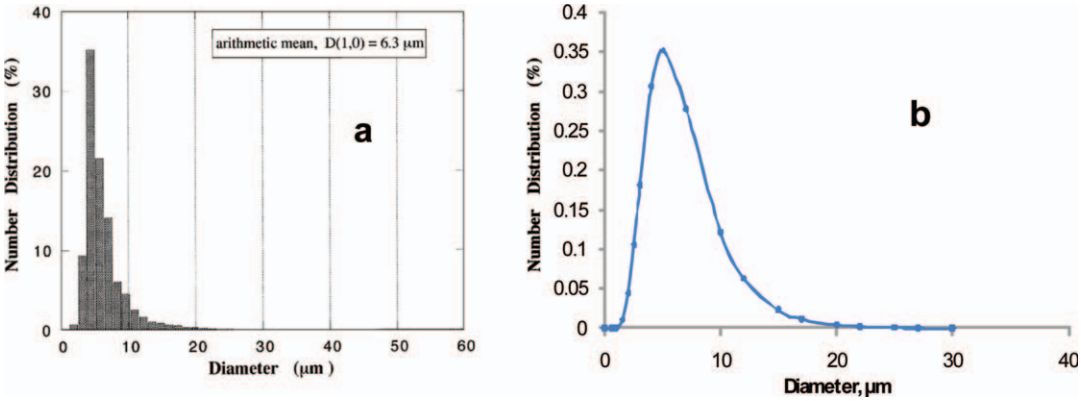

Figure 2. (a) Experimental bubble size distribution[18] and (b) log-normal distribution using μ and σ values of 0.8 and 0.04, respectively.

[Color figure can be viewed in the online issue, which is available at wileyonlinelibrary.com.]

the type of ultrasonic generator used by them (a 20-kHz immersion horn) are very similar to the system we used. Their experimental data on bubble size distribution are, therefore, used for the determination of the number of bubbles and the rate of generation of ·OH radicals. It was observed that the bubble size distribution they found follows the shape of a log-normal distribution. The following expression corresponding to a log-normal distribution

$$N(R_0;\eta,\sigma) = \frac{1}{R_0\sigma\sqrt{2\pi}} e^{-\frac{(\ln(R_0)-\eta)^2}{2\sigma^2}} \tag{31}$$

has been fitted to their data and the coefficients η (mean) and σ (standard deviation) have been found to be 0.8 and 0.04, respectively. Figure 2 shows the experimental data and the corresponding log-normal distribution. Using this functional form of bubble size distribution, we can find a single average bubble volume ($\langle V\rangle_{t,R_0}$) and a single rate of dissolution of ·OH radicals ($\langle r_{\mathrm{d,OH}}\rangle_{t,R_0}$) according to the following expressions

$$\langle r_{\mathrm{d,OH}}\rangle_{t,R_0} = \frac{\int_{R_0(\mathrm{lower})}^{R_0(\mathrm{higher})} N(R_0)(r_{\mathrm{d,OH}})_t dR_0}{\int_{R_0(\mathrm{lower})}^{R_0(\mathrm{higher})} N(R_0) dR_0} \tag{32}$$

$$\langle V\rangle_{t,R_0} = \frac{\int_{R_0(\mathrm{lower})}^{R_0(\mathrm{higher})} N(R_0)(V)_t dR_0}{\int_{R_0(lower)}^{R_0(\mathrm{higher})} N(R_0) dR_0} \tag{33}$$

The number of bubbles has been estimated from the void fractions calculated in Tsochatzidis et al.[18] The range of void fractions calculated is between 10^{-3} and 10^{-4}. We use these two values to calculate the upper and lower limits of the total number of bubbles according to the following

$$N = \frac{\epsilon}{(V(R_0))_t} \tag{34}$$

where ϵ is the void fraction and N is the number of bubbles per unit volume. Once this is calculated, the average rate of generation of ·OH radicals in the reactor can be given by the expression

$$S_{\mathrm{OH}} = \langle r_{\mathrm{d,OH}}(R_0)\rangle_t N \tag{35}$$

Transfer of NO from flowing gas phase

The transport of NO from gas to liquid phase has been treated according to the film theory of gas-liquid absorption. As NO is very sparingly soluble in water, the mass transfer is assumed to be entirely controlled by the liquid film. The mass-transfer coefficient is calculated from correlations in literature applicable to bubble columns. From mass-transfer correlations available in the literature[69,70] for small bubbles (<2.5 mm)

$$k_{\mathrm{L}}(N_{Sc})^{\frac{2}{3}} = 0.31\left(\frac{\Delta\rho\mu_{\mathrm{c}}g}{\rho_{\mathrm{c}}^2}\right)^{\frac{1}{3}} \tag{36}$$

where k_L is the mass-transfer coefficient, μ_c and ρ_c are viscosity and density of the condensed phase (here water), $\Delta\rho$ is the density difference between the phases, and g is the gravitational acceleration. N_{Sc} is the Schmidt number which is given by

$$N_{Sc} = \frac{\mu_{\mathrm{c}}}{\rho_{\mathrm{c}}D_{\mathrm{L}}} \tag{37}$$

A more accurate correlation (by Calderbank and Moo-Young[69]) is

$$N_{Sh} = 2 + 0.31N_{Ra}^{\frac{1}{3}} \tag{38}$$

N_{Sh} is the Sherwood number and is given by

$$N_{Sh} = \frac{k_{\mathrm{L}}d_{\mathrm{B}}}{D_{\mathrm{L}}} \tag{39}$$

where d_g is the bubble diameter. N_{Ra} is the Rayleigh number (mass) and is given by

$$N_{Ra} = N_{Gr}N_{Sc} \tag{40}$$

where N_{Gr} is the Grasshof number (mass)

$$N_{Gr} = \frac{\rho_{\mathrm{c}}g\Delta\rho d_{\mathrm{B}}^3}{\mu_{\mathrm{c}}^2} \tag{41}$$

The interfacial area has been obtained from Adewuyi and Owusu[71] who have worked on the same NO removal system using the same configuration of a bubble column reactor.

Solution method

Equations 1, 11, and 22 coupled with the system of differential equations for reaction kinetics corresponding to Eq. 27 constitute the model for a single bubble sonochemistry. They are solved in the following way. The first three equations are solved with Runge–Kutta fourth-order adaptive step-size solver and at each time step the kinetic equations are solved using Runge–Kutta second-order solver to get the composition of the bubble which are then fed into the first set of equations. The software used for the numerical simulations is Matlab.

Results and Discussion

The bubble dynamics equations have been used to generate information such as bubble volume vs. time and number of reactive radicals vs. time. These data and the estimated number of bubbles allow us to calculate the rate of generation of ·OH radicals per unit time per unit volume. The illustrative results from the cavitation model simulations are shown in Figure 3. The conditions used for these simulations are taken from Didenko and Suslick[44] to be able to validate our results against theirs. For the validation, we have compared our results against those found experimentally by the same researchers[44] and those from a more detailed model by Yasui et al.[24] with conditions: $f = 52$ kHz, $P_A = 1.52$ bar, $T_{amb} = 276$ K, $P_h = 1$ atm, and $R_0 = 4$ μm. The yields of photons or the number of molecules (·OH and NO_2^-) per acoustic cycle per pressure are given in Table 4.

Reasonable agreement is obtained between the experimental ·OH radical generation value and our model prediction. The values of other important species are also close to the model predictions by the diffusion-limited model and the model by Yasui et al.[24] On the other hand, there is a large difference between the HNO_2 values obtained by our model and experiment and other models. This could be accounted for by the fact that we neglected the diffusion of dissolved air into the bubble due to the reasons discussed earlier. These simulations were done with a constant initial composition of the bubble of 95% Ar, and equal proportions of N_2 and O_2 for the balance. Some variations of our model results from other models and experimental results are expected due to various other simplifications in our model to decrease computation time and due to the large uncertainty of the physical and kinetic parameters used. However, it should be noted that this does not influence the significance of our results which are qualitative in nature as will be evident later. In addition, the calculated ·OH radicals are a conservative one instead of an optimistic one. Also, for the next simulations, we will be using the assumption of an air bubble with constant initial composition instead of an SBSL bubble which contains mainly Ar.

The most important parameters of interest for our simulations are the initial bubble radius and the acoustic pressure amplitude; the frequency is assumed to be the same as the driving frequency of 20 kHz. Determination of the bubble radius is not as straight forward as in the single bubble case, as there is a large number and different sizes of cavitation bubbles present. We use the data from Tsochatzidis et al.,[18] who have used reactor geometries and ultrasonic generator (a 20-kHz immersion horn) very similar to our system. Among other things, they have shown that the mean bubble diameter is not very much dependent on the ultrasonic power input, therefore, a mean size of 5 μm is taken following their data as the initial bubble radius for our simulations.

As has already been pointed out, because of attenuation by the bubbles themselves, the ultrasonic pressure amplitude decreases through the reactor and the actual pressure felt by a bubble is different depending on the location of the reactor. The pressure amplitude generated at the horn tip is given by the expression

$$P_A = \sqrt{2\rho v I} \tag{42}$$

where v is the velocity of sound in water and I is the intensity at the horn tip. For a power input of 70 W, the pressure at the horn tip becomes about 12.4 atm. This is a very high forcing and there is vigorous cavitation activity near the horn tip, eventually the tip gets pitted due to the cavitation there. However, because of the extreme cavitational activity near the horn, the attenuation is also high. Cavitation activity is not very prominent at the bottom of the reactor, that is, far from the horn. McNamara et al.[72] experimentally measured the temperatures for MBSL and found the maximum temperature to be in the order of 5000 K. Also, Yasui et al.[73] discussed the optimum temperature for the production of oxidants from a modeling perspective and found that it is about 5500 K for nitrogen containing bubbles. The corresponding acoustic amplitude found by Yasui et al.[73] was 2.2 atm at 140 kHz. In our simulations, this temperature was reached for an amplitude of 2 atm for an air bubble. In another article, Yasui[23] scanned the $R_0 - P_A$ parameter space of MBSL for stability. It is shown that for a frequency of 20 kHz and initial radius of 5 μm, unstable sonoluminescing bubbles (fragmentary transient cavitation) occur, which is our assumption for the dominant cavitational phenomena occurring in the reactor, for pressure amplitude of 2 bar. Therefore, acoustic amplitude of 2 bar is assumed for our subsequent simulations.

From the results of the simulation, the average volume of a cavitation bubble, $\langle V(R_0)\rangle_t = 3.51 \times 10^{-12}\text{m}^3$ and rate of dissolution of ·OH radicals, $\langle r_{d,OH}(R_0)\rangle_t = 8.33 \times 10^{10}$ molecules/s. Therefore, the range of number of bubbles: $N = 2.85 \times 10^7$ to 1.42×10^9 bubbles/m^3 and the corresponding rate of generation of ·OH radicals: $S_{OH} = 8.14 \times 10^{-9}$ to 4.07×10^{-7} mol/(L s).

The balance equations for the different species in the bubble column are[74]

$$\frac{dC^g_{NO}}{dt} = \frac{Q^g}{V_g}\left(C^g_{NO(in)} - C^g_{NO}\right) - \frac{V_l}{V_g}k_L a\left(C^g_{NO,i} - C^l_{NO}\right) \tag{43}$$

$$\frac{dC^l_{NO}}{dt} = k_L a\left(C^g_{NO,i} - C^l_{NO}\right) - r_{OH} \tag{44}$$

$$\frac{dC_{OH}}{dt} = S_{OH} - r_{OH} \tag{45}$$

where in general $C^p_{x,i}$ denotes concentration of species x in phase g and i implies interfacial; and similar equations for other species in Table 3.

Simulations for NO absorption

We are simulating a semibatch system for the absorption of NO. The gas phase is flowing continuously and the liquid

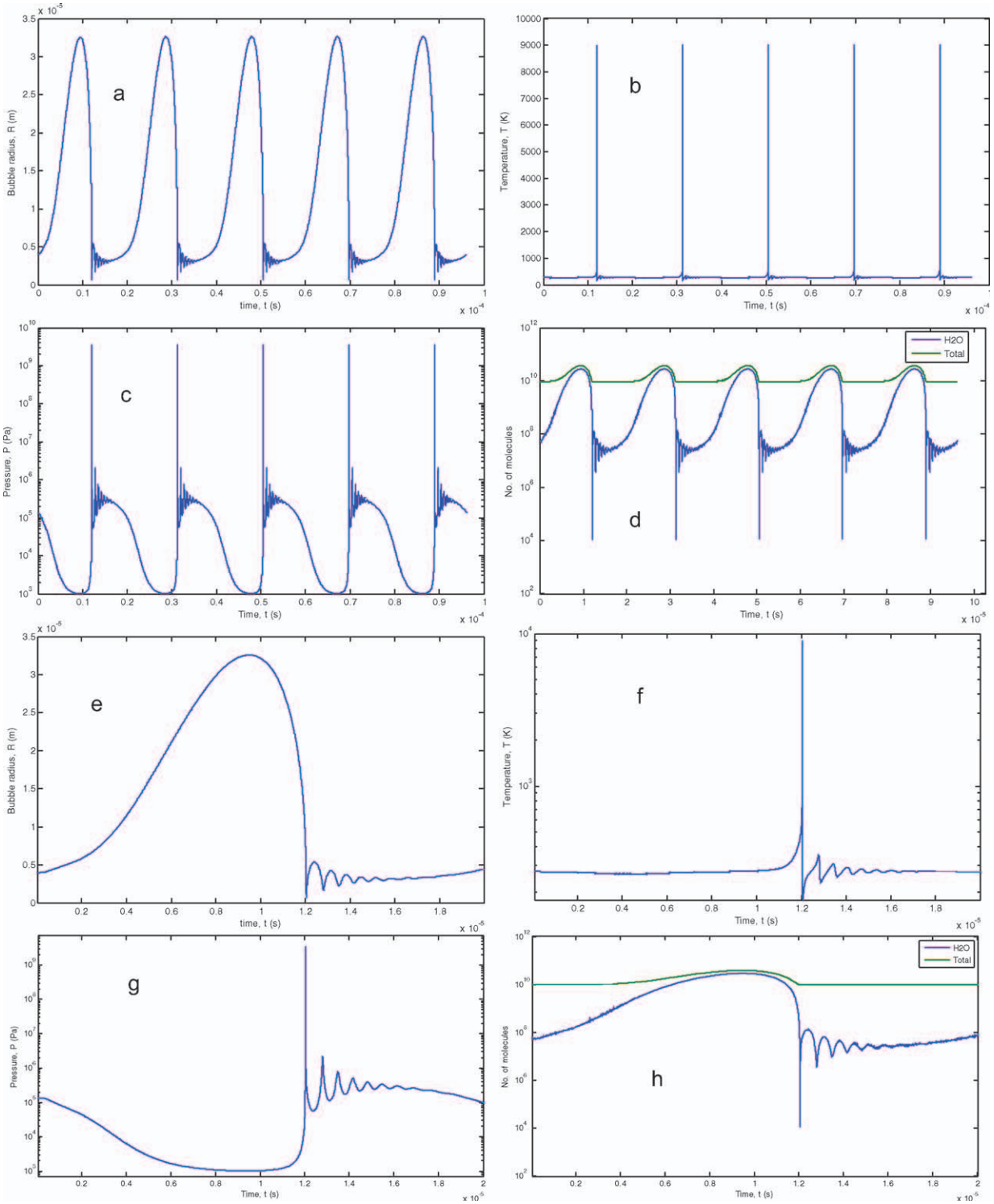

Figure 3. Cavitation model simulation results.

Simulation conditions: $f = 52$ kHz, $P_A = 1.52$ bar, $T_{amb} = 276$ K, $P_h = 1$ atm, and $R_0 = 4$ μm. (a) Radius vs. time (five acoustic cycles), (b) temperature vs. time (five acoustic cycles), (c) pressure vs. time (five acoustic cycles), (d) no. of molecules vs. time (five acoustic cycles), (e) radius vs. time (one acoustic cycle), (f) temperature vs. time (one acoustic cycle), (g) pressure vs. time (one acoustic cycle), and (h) no. of molecules vs. time (one acoustic cycle). [Color figure can be viewed in the online issue, which is available at wileyonlinelibrary.com.]

phase is constant, with the ultrasonic probe dipped into it. The following are the global variables that are used for the simulations corresponding to the experiments. They remain constant for all the simulations.

Gas flow rate $Q^g = 0.1$ slpm $= 1.667$ cm^3/s. Liquid volume $V^l = \frac{\pi}{4}D^2h = \frac{\pi}{4} \times 10^2 \times 16 = 1256.64$ cm^3. Gas holdup $V^g = \frac{\pi}{4}D^2h = \frac{\pi}{4} \times 10^2 \times 1 = 78.54$ cm^3 (assuming a height increment of 1 cm). Henry's law constant for NO $H_{NO} = 5.1546 \times 10^5$atm/(mol/cm^3).

The initial simulation of NO absorption was done using a generation of ·OH radicals equal to lower limit of the range 8.14×10^{-9}mol/Ls and the calculated value of volumetric

Table 4. Comparison of the Results Obtained Using Our Model with Those of Experiment and Other More Detailed Model

				Present Model
	Experiment[44]	Yasui et al.[24]	Diffusion Limited[24]	95% Ar, 2.5% N_2, and 2.5% O_2
T_{max} (K)	–	10,900	9400	10,200
Photon	7.5×10^4	8.0×10^4	4.9×10^4	–
OH	8.2×10^5	6.6×10^5	9.2×10^5	1.1841×10^5
O	–	1.3×10^7	1.1×10^7	1.9562×10^7
H_2O_2	–	6.3×10^6	9.2×10^6	2.6197×10^6
O_3	–	3.4×10^4	4.0×10^4	3.1830×10^4
HNO_2 (NO_2^-)	9.9×10^6	2.3×10^6	2.0×10^6	6.3503×10^1
HNO_3	–	8.4×10^5	–	2.1077×10^4

Data are given as yields of photons or number of molecules per acoustic cycle.

or global mass-transfer coefficient $k_La = 1.57 \times 10^{-2}s^{-1}$. Using these data, the results of the simulation which also take into consideration size distribution of bubble in the presence of ultrasound discussed earlier, are shown in Figure 4.

Figure 4a shows that the conversion of NO reaches ~20% and then starts to decrease and eventually reaches very low value. Comparing this with the ·OH radical concentration we can see that it reaches about 2×10^{-7} mmol/L and then decreases to negligible proportions. This means that there are not enough ·OH radicals available for reaction with NO. The reason for this is that at this rate of generation, the other competing reactions for ·OH radicals (chiefly Reactions 2 and 3 in Table 3) become important and consume ·OH at a rate higher than it is supplied. It is evident from the H_2O_2 profile that both Reactions 2 and 3 eventually proceed at the same rate because the concentration of H_2O_2 reaches a steady-state after some time. These reactions consume three molecules of ·OH for each molecule of $O_2{\cdot}^-$ produced. It must be remembered that this rate of H_2O_2 generation does not include the H_2O_2 generated in the cavitation bubbles and dissolved into the liquid. That term would actually make the H_2O_2 concentration increase with time but it has been disregarded for simplicity. Hence, at this level of generation of ·OH radicals, it becomes the controlling factor for the absorption for NO.

Figure 5 shows the effect of increasing the rate of ·OH radical generation to the higher limit calculated (i.e., $S_{OH} = 4.07 \times 10^{-7}$mol/(Ls)) keeping k_La the same. We can observe immediately the effect of increase in ·OH radical generation. The fractional conversion of NO has increased and reached a steady-state, which indicates that it is consumed at the rate it enters the liquid phase. This means that there are enough ·OH radicals available to effect the oxidation of NO and keep the driving force for its absorption. Although the recombination reaction and other competing reactions play a role in keeping the level of ·OH radical concentration down, however, they are not as significant as they

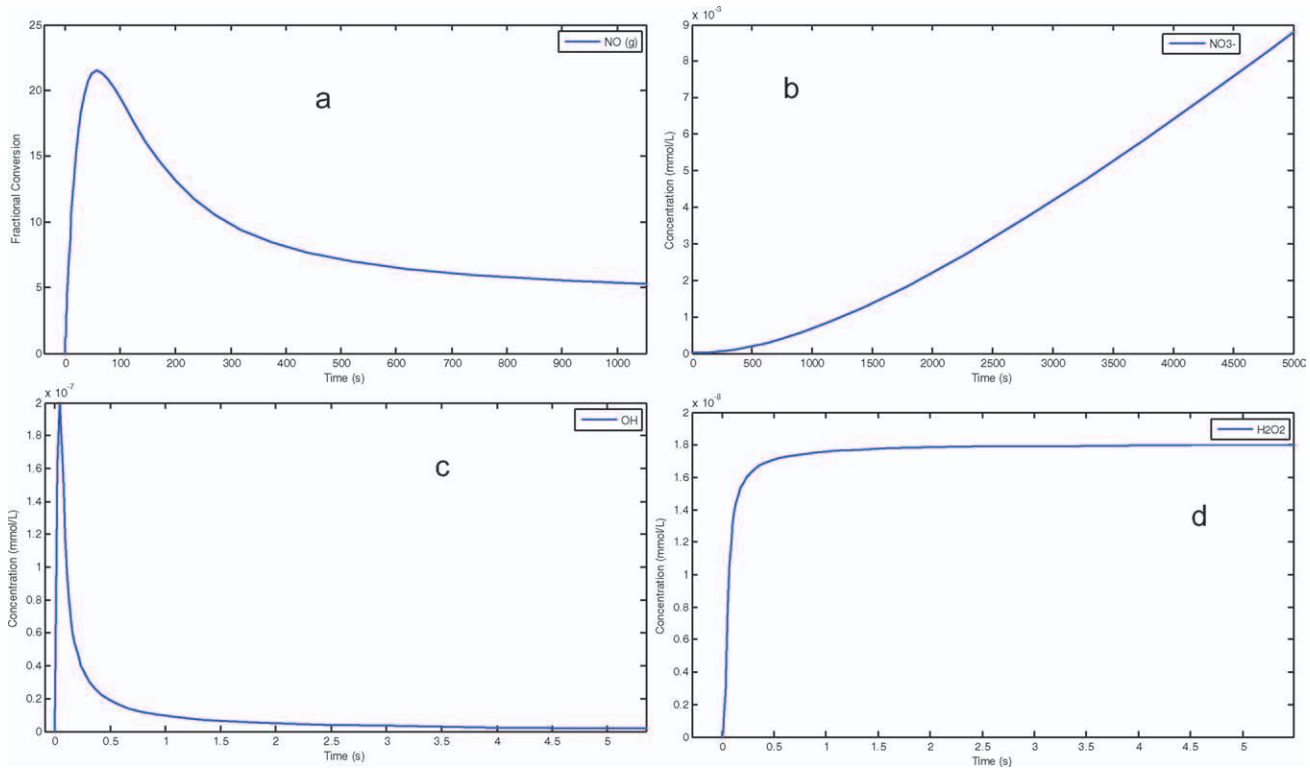

Figure 4. NO absorption simulation 1.

(a) NO fractional conversion vs. time, (b) NO_3^- concentration vs. time, (c) ·OH concentration vs. time, and (d) H_2O_2 concentration vs. time. [Color figure can be viewed in the online issue, which is available at wileyonlinelibrary.com.]

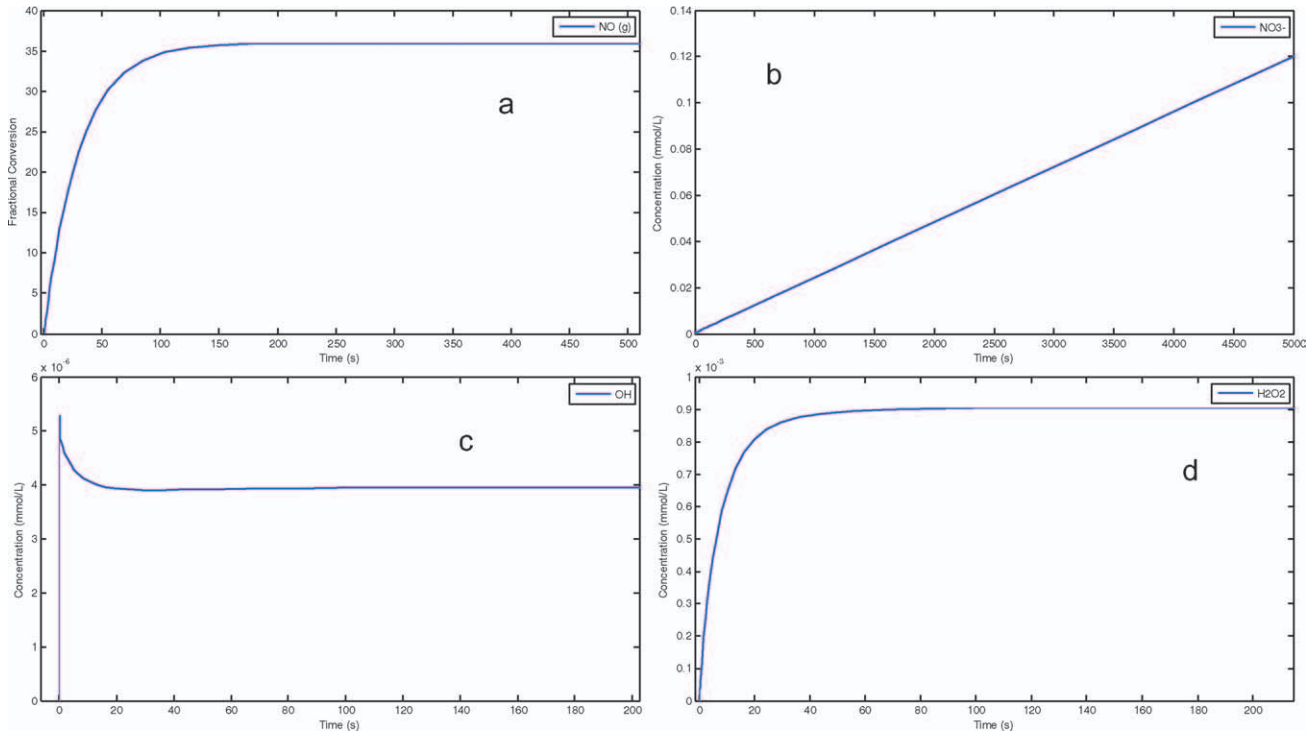

Figure 5. NO absorption simulation 2.

(a) NO fractional conversion vs. time, (b) NO_3^- concentration vs. time, (c) ·OH concentration vs. time, and (d) H_2O_2 concentration vs. time. [Color figure can be viewed in the online issue, which is available at wileyonlinelibrary.com.]

were in the previous case. The steady-state concentration is about an order-of-magnitude higher than the previous case. At this level, the mass transfer becomes the controlling mechanism.

The data from NO absorption experiment are presented in Figure 6. The steady-state fractional conversion is about 78%. The initial jump in fractional conversion is due to the initial mixing of the incoming gas (containing NO) with that over the liquid surface. To match the model prediction with the experiment, one further simulation was done where the mass-transfer coefficient was increased to five times the previous value used. The results are shown in Figure 7. Figure 7a shows the effect of increasing the mass-transfer on NO fractional conversion. It is obvious from this figure that the fractional conversion reaches a steady-state at about 75%. The ·OH radical profile in Figure 7b shows a different kind of behavior this time; it decreases to a very low value and then increases again to level off about 3.2×10^{-6} mmol/L. This is lower than the steady-state of 4×10^{-6} mmol/L reached in the previous simulation (Figure 5c). Evidently, this is due to the increased consumption rate by the NO, more of which now enters from the gas phase. The initial dip in Figure 7b is attributed to the fact that, initially there is very little ·OH radicals present and its amount depletes more quickly due to the enhanced transfer of NO. Finally, because of the decrease of NO transfer rate and ·OH radical's continuous supply, the concentration of ·OH increases. This could be visualized well from the profile of aqueous NO in Figure 7c. The amount of dissolved NO increases with time until its reaction with ·OH radicals (shown in Figure 7b) becomes significant due to the latter's increased abundance, bringing the concentration of dissolved NO down to an insignificant value (Figure 7c).

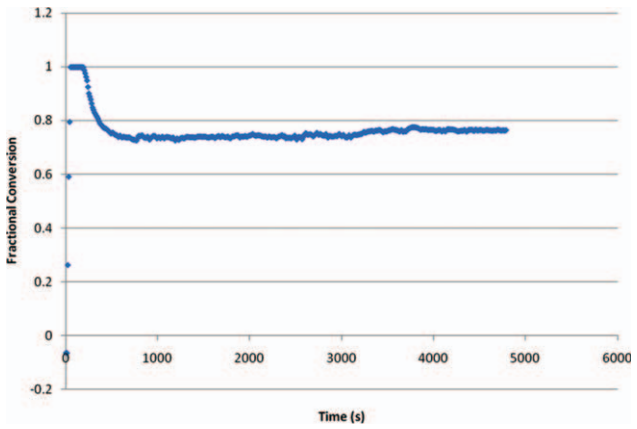

Figure 6. Experimental data of NO absorption,[5,6] the axis has been changed from NO concentration vs. time in the original data to NO fractional conversion vs. time.

Conditions of experiment: NO concentration = 1000 ppm, ultrasonic power = 110 W, liquid volume = 1200 ml, no buffer, and pH = 6.8–6.0. [Color figure can be viewed in the online issue, which is available at wileyonlinelibrary.com.]

In addition to the reaction enhancement causing greater driving force for mass transfer, ultrasound enhances mass transfer through a couple of other mechanisms. Olson and Barbier[1] reported an apparent mass-transfer coefficient of O_3 of 57% higher in the presence of ultrasound (power input of 54 W) than without (0.44 vs. 0.28 min^{-1}) and suggested the enhancement to be due to mechanical effects such as acoustic streaming (mixing) and ultrasonic breakup of gas bubbles entering the reactor. Acoustic streaming is caused by an energy gradient in the direction of propagation of the

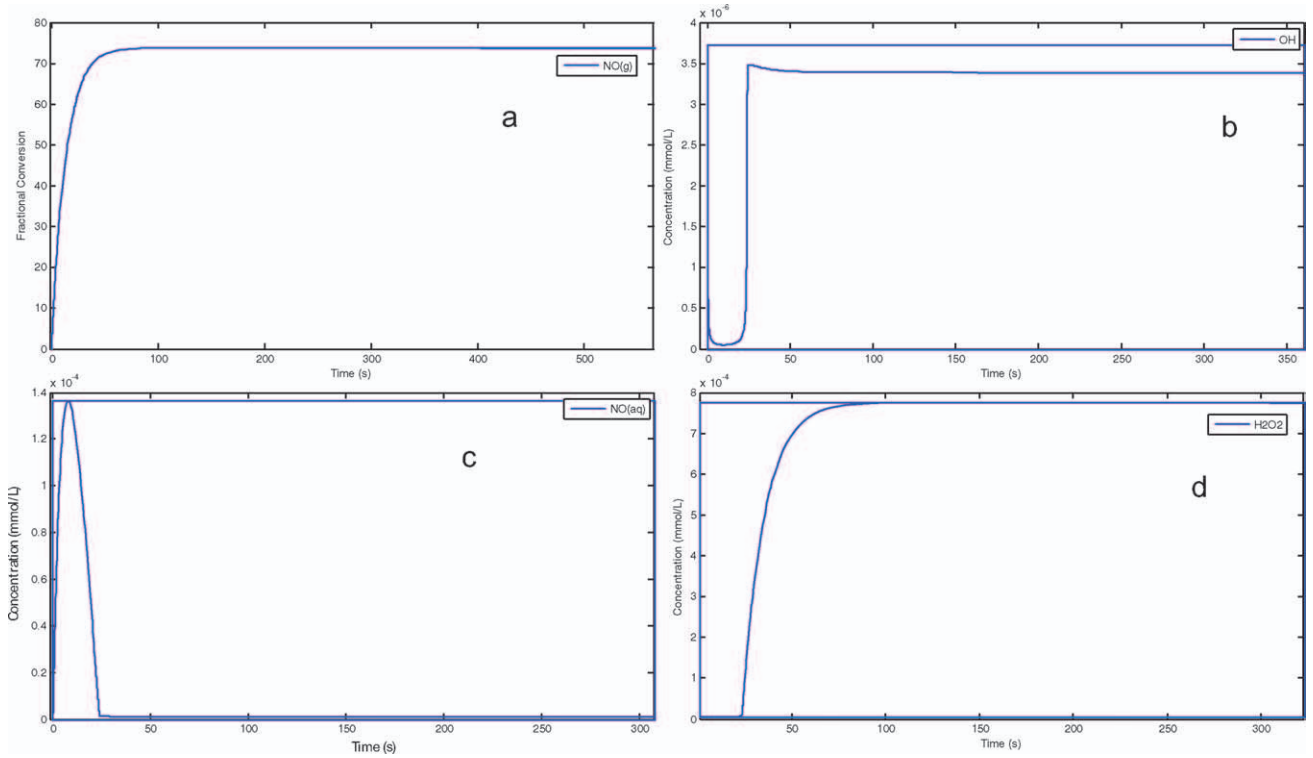

Figure 7. NO absorption simulation 3.

(a) NO fractional conversion vs. time, (b) ·OH concentration vs. time, (c) aqueous NO concentration vs. time, and (d) H_2O_2 concentration vs. time. [Color figure can be viewed in the online issue, which is available at wileyonlinelibrary.com.]

acoustic wave. The energy gradient corresponds to a force which when acting on a liquid causes the liquid to accelerate. The greater mixing due to turbulence created by acoustic streaming reduces the liquid film thickness. According to the two-film theory, liquid side mass-transfer coefficient is inversely proportional to the liquid film thickness. The decrease in liquid film thickness would result in the increase of k_L. Also, the breakup of gas bubbles increases the specific interfacial area, a_A. Therefore, the volumetric mass-transfer coefficient, $k_L a_A$ would increase in the presence of ultrasound. Weavers and Hoffmann[2] performed mass-transfer studies of ozone in aqueous solution open to the atmosphere, closed to the atmosphere and open to the atmosphere with ozone gas bubbling in 20- and 500-kHz system. They concluded that ozone mass transfer was enhanced by ultrasonic irradiation and indicated that the effect was due to both mechanical effects and to the decreased concentration of ozone in the liquid phase. They also found that acoustic streaming was much greater at 20 kHz than at 500 kHz. Zhang et al.[3] also measured ozone mass transfer using a different technique and came up with similar conclusions.

Laugier et al.[4] recently conducted thorough mass-transfer studies of nitrogen in the presence of ultrasound and mechanical stirring. They obtained almost an order-of-magnitude enhancement in mass-transfer coefficient in the range that we have used in our model. Their system is different from ours in that they have a gas-inducing turbine and higher pressure for the gassing-in experiments. It is expected that gas bubbling will induce mixing similar to that obtained in a stirrer and as the bubbles introduced in our column are very small (<1 mm), there should be a high interfacial area available for mass transfer. Also, a driving force will be always present due to the constant consumption of the aqueous or dissolved NO in the liquid phase. Therefore, the mass-transfer coefficients without ultrasound for these two systems should be comparable. From our results, it is seen that the effect of ultrasound is mainly on the mass-transfer coefficient. We have shown here by a detailed modeling that, for example, a five-fold enhancement of mass transfer for NO absorption with ultrasound is possible and that this effect is mainly due to the mechanical agitation introduced by ultrasound in a liquid medium, as the chemistry induced by acoustic cavitation is inadequate to explain the amount of conversion obtained experimentally.

Conclusion

A sonochemical bubble column for the absorption of NO was modeled. Bubble dynamics simulations of acoustic cavitation, incorporating liquid compressibility, mass and heat transport, and chemical reaction, were performed. Coupling the chemistry generated from these microscopic phenomena to the reaction occurring in the liquid phase and mass transfer from the gas phase, the fractional conversion of NO was obtained. The results of the simulations indicate that sonochemical oxidation alone cannot explain the previously reported experimental results of NO removal by ultrasonic cavitation. Further simulations, with higher mass-transfer coefficients (equivalent to those found by other investigators in presence of ultrasound), show that only a combination of chemical activity and mass-transfer enhancement by ultrasound (turbulence and microstreaming) can explain the results obtained. A complete analysis and prediction of the rates of sonochemical reacting systems and sonochemical oxidations of pollutants or other substrates still requires many efforts on the theoretical aspects (validity of many

assumptions, thermodynamics at high-temperatures and pressures, fast reaction kinetics for radical formation, free radicals transport to the liquid phase, estimation or quantification of liquid-phase mass-transfer coefficients); incorporation of growth/dissolution by rectified diffusion; bubble movement by radiation force and buoyancy; and cavitation bubble population for which there are more recent advances as noted earlier. Thus, the present model provides a framework for these complex systems on which more robust and rigorous models coupling bubble dynamics with mass transfer and chemical/cavitational reaction kinetics can be developed for various cavitational gas-liquid systems and reactors.

Therefore, our current and future efforts are concentrated on gathering more experimental data to validate, critically evaluate and improve the model using ultrasonic reactors of different geometries and spatial variation of cavitational activities. Working with Advanced Sonic Processing Systems (Advanced Sonics, LLC, Oxford, CT) we have designed, built, and assembled a new ultrasonic gas-liquid reactor with more uniform ultrasonic power distribution for further studies. The next generation of models will also allow the determination of optimal operating regions in terms of physical–chemical parameters. Research on the quantification of the mass-transfer rates—the all important information in the efficient design of coupled gas-liquid sonochemical system, is still in its infantile stage.[75] More detailed laboratory-scale investigations to improve our understanding of the extent of mass-transfer intensification resulting from ultrasonic irradiation as a function of process and operating parameters will be undertaken.

Acknowledgments

The authors acknowledge the funding received from National Science Foundation (NSF) for the financial assistance via Award No. Grant CBET-0651811. They also thank Samuel O. Owusu for the experimental data obtained while pursuing his Master's degree at North Carolina Agricultural and Technical State University.

Literature Cited

1. Olson T, Barbier P. Oxidation kinetics of natural organic matter by sonolysis and ozone. *Water Res (Oxford)*. 1994;28:1383–1391.
2. Weavers L, Hoffmann M. Sonolytic decomposition of ozone in aqueous solution: mass transfer effects. *Environ Sci Technol*. 1998;32:3941–3947.
3. Zhang H, Duan L, Zhang D. Absorption kinetics of ozone in water with ultrasonic radiation. *Ultrason Sonochem*. 2007;14:552–556.
4. Laugier F, Andriantsiferana C, Wilhelm A, Delmas H. Ultrasound in gas–liquid systems: effects on solubility and mass transfer. *Ultrason Sonochem*. 2008;15:965–972.
5. Owusu S, Adewuyi Y. Sonochemical removal of nitric oxide from flue gases. *Ind Eng Chem Res*. 2006;45:4475–4485.
6. Adewuyi Y, Owusu S. Ultrasound-induced aqueous removal of nitric oxide from flue gases: effects of sulfur dioxide, chloride, and chemical oxidant. *J Phys Chem A*. 2006;110:11098–11107.
7. Adewuyi Y. Sonochemistry: environmental science and engineering applications. *Ind Eng Chem Res*. 2001;40:4681–4715.
8. Ciawi E, Rae J, Ashokkumar M, Grieser F. Determination of temperatures within acoustically generated bubbles in aqueous solutions at different ultrasound frequencies. *J Phys Chem B*. 2006;110:13656–13660.
9. Adewuyi YG, Appaw C. Sonochemical oxidation of carbon disulfide in aqueous solutions: reaction kinetics and pathways. *Ind Eng Chem Res*. 2002;41:4957–4964.
10. Appaw C, Adewuyi YG. Destruction of carbon disulfide in aqueous solutions by sonochemical oxidation. *J Hazard Mater*. 2002;90:237–249.
11. Kotronarou A, Mills G, Hoffmann M. Ultrasonic irradiation of *p-nitrophenol in aqueous solution. J Phys Chem*. 1991;95:3630–3638.
12. Hart E, Henglein A. Sonochemistry of aqueous solutions: H_2O_2 combustion in cavitation bubbles. *J Phys Chem*. 1987;91:3654–3656.
13. Hua I, Hoechemer R, Hoffmann M. Sonolytic hydrolysis of *p-nitrophenyl acetate: the role of supercritical water*. *J Phys Chem*. 1995;99:2335–2342.
14. Hart E, Henglein A. Sonolysis of ozone in aqueous solution. *J Phys Chem*. 1986;90:3061–3062.
15. Hart E, Henglein A. Sonolytic decomposition of nitrous oxide in aqueous solution. *J Phys Chem*. 1986;90:5992–5995.
16. Hart E, Fischer C, Henglein A. Pyrolysis of acetylene in sonolytic cavitation bubbles in aqueous solution. *J Phys Chem*. 1990;94:284–290.
17. Kotronarou A, Hoffmann MR.*The chemical effects of collapsing cavitation bubbles: mathematical modeling*. In: Huang CP, O'Melia CR, Morgan JJ, editors. *Advances in Chemistry Series 244*. Washington, DC: American Chemical Society, 1995.
18. Tsochatzidis N, Guiraud P, Wilhelm A, Delmas H. Determination of velocity, size and concentration of ultrasonic cavitation bubbles by the phase-Doppler technique. *Chem Eng Sci*. 2001;56:1831–1840.
19. Gogate PR, Tatake PA, Kanthale PM, Pandit AB. Mapping of sonochemical reactors: review, analysis, and experimental verification. *AIChE J*. 2002;48:1542–1560.
20. Dähnke S, Keil FJ. Modeling of three-dimensional linear pressure fields in sonochemical reactors with homogeneous and inhomogeneous density distributions of cavitation bubbles. *Ind Eng Chem Res*. 1998;37:848–864.
21. Gaitan DF, Crum LA, Church CC, Roy RA. Sonoluminescence and bubble dynamics for a single, stable, cavitation bubble. *J Acoust Soc Am*. 1992;91:3166–3183.
22. Yasui K. Effect of volatile solutes on sonoluminescence. *J Chem Phys*. 2002;116:2945–2954.
23. Yasui K. Influence of ultrasonic frequency on multibubble sonoluminescence. *J Acoust Soc Am*. 2002;112:1405–1413.
24. Yasui K, Tuziuti T, Sivakumar M, Iida Y. Theoretical study of single-bubble sonochemistry. *J Chem Phys*. 2005;122:224706-1–224706-12.
25. Kondic L, Yuan C, Chan CK. Ambient pressure and single-bubble sonoluminescence. *Phys Rev E*. 1998;57:R32–R35.
26. Puente GF, Urteaga R, Bonetto FJ. Numerical and experimental study of dissociation in an air–water single-bubble sonoluminescence system. *Phys Rev E*. 2005;72:046305-1–046305-10.
27. Suslick KS. *Sonoluminescence and sonochemistry*. In: Meyers RA, editor. *Encyclopedia of Physical Science and Technology*, 3rd ed. San Diego: Academic Press, Inc., 2001.
28. Storey BD, Szeri AJ. A reduced model of cavitation physics for use in sonochemistry. *Proc R Soc Lond Ser A: Math Phys Eng Sci*. 2001;457:1685–1700.
29. Suslick KS, Didenko Y, Fang MM, Hyeon T, Kolbeck KJ, McNamara WB, Mdleleni MM, Wong M. Acoustic cavitation and its chemical consequences. *Philos Trans R Soc Lond Ser A: Math Phys Eng Sci*. 1999;357:335–353.
30. Storey BD, Szeri AJ. Argon rectification and the cause of light emission in single-bubble sonoluminescence. *Phys Rev Lett*. 2002;88:074301-1–074301-3.
31. Sivasankar T, Moholkar V. Physical features of sonochemical degradation of nitroaromatic pollutants. *Chemosphere*. 2008;72:1795–1806.
32. Sivasankar T, Moholkar V. Mechanistic features of the sonochemical degradation of organic pollutants. *AIChE J*. 2008;54:2206–2219.
33. Sivasankar T, Paunikar A, Moholkar V. Mechanistic approach to enhancement of the yield of a sonochemical reaction. *AIChE J*. 2007;53:1132–1143.
34. Prosperetti A, Lezzi A. Bubble dynamics in a compressible liquid. Part 1. First-order theory. *J Fluid Mech*. 1986;168:457–478.
35. Yasui K. A new formulation of bubble dynamics for sonoluminescence. *Electron Commun Jpn Part II: Electron*. 1998;81:39–45.
36. Putterman SJ, Weninger KR. Sonoluminescence: how bubbles turn sound into light. *Ann Rev Fluid Mech*. 2000;32:445–476.
37. Walton AJ, Reynolds GT. Sonoluminescence. *Adv Phys*. 1984;33:595–660.
38. Prosperetti A, Crum LA, Commander KW. Nonlinear bubble dynamics. *J Acoust Soc Am*. 1988;83:502–514.
39. Kamath V, Prosperetti A, Egolfopoulos FN. A theoretical-study of sonoluminescence. *J Acoust Soc Am*. 1993;94:248–260.
40. Sivasankar T, Moholkar VS. Physical insights into the sonochemical degradation of recalcitrant organic pollutants with cavitation bubble dynamics. *Ultrason Sonochem*. 2009;16:769–781.
41. Kalva A, Sivasankar T, Moholkar VS. Physical mechanism of ultrasound-assisted synthesis of biodiesel. *Ind Eng Chem Res*. 2008;48:534–544.
42. Yasui K. Alternative model of single-bubble sonoluminescence. *Phys Rev E*. 1997;56:6750–6760.
43. Brenner M, Hilgenfeldt S, Lohse D. Single-bubble sonoluminescence. *Rev Modern Phys*. 2002;74:425–484.
44. Didenko Y, Suslick K. The energy efficiency of formation of photons, radicals and ions during single-bubble cavitation. *Nature*. 2002;418:394–397.

45. Fujikawa S, Akamatsu T. Effects of the non-equilibrium condensation of vapour on the pressure wave produced by the collapse of a bubble in a liquid. *J Fluid Mech Digital Arch.* 1980;97:481–512.
46. Yasui K. Effects of thermal conduction on bubble dynamics near the sonoluminescence threshold. *J Acoust Soc Am.* 1995;98:2772–2782.
47. Akhatov I, Lindau O, Topolnikov A, Mettin R, Vakhitova N, Lauterborn W. Collapse and rebound of a laser-induced cavitation bubble. *Phys Fluids.* 2001;13:2805–2819.
48. Li Y, Davidovits P, Shi Q, Jayne J, Kolb C, Worsnop D. Mass and thermal accommodation coefficients of H_2O (g) on liquid water as a function of temperature. *J Phys Chem A.* 2001;105:10627–10634.
49. Lin S. Non-equilibrium phase change. *Interfacial Fluid Dyn Transp Proc.* 2003;628:355–367.
50. Ytrehus T, Østmo S. Kinetic theory approach to interphase processes. *Int J Multiphase Flow.* 1996;22:133–155.
51. Schrage R, *A Theoretical Study of Interphase Mass Transfer*. New York: Columbia University Press, 1953.
52. Young FR. Sonoluminescence from water containing dissolved gases. *J Acoust Soc Am.* 1976;60:100–104.
53. Barber BP, Putterman SJ. Light scattering measurements of the repetitive supersonic implosion of a sonoluminescing bubble. *Phys Rev Lett.* 1992;69:3839–3842.
54. Toegel R, Lohse D. Phase diagrams for sonoluminescing bubbles: a comparison between experiment and theory. *J Chem Phys.* 2003; 118:1863–1875.
55. Sochard S, Wilhelm A, Delmas H. Gas–vapour bubble dynamics and homogeneous sonochemistry. *Chem Eng Sci.* 1998;53:239–254.
56. Naidu DVP, Rajan R, Kumar R, Gandhi KS, Arakeri VH, Chandrasekaran S. Modelling of a batch sonochemical reactor. *Chem Eng Sci.* 1994;49:877–888.
57. Rajan R, Kumar R, Gandhi KS. Modelling of sonochemical oxidation of the water–KI–CCl_4 system. *Chem Eng Sci.* 1998;53:255–271.
58. Colussi A, Weavers L, Hoffmann M. Chemical bubble dynamics and quantitative sonochemistry. *J Phys Chem A.* 1998;102:6927–6934.
59. Storey B, Szeri A. Water vapour, sonoluminescence and sonochemistry. *Proc: Math Phys Eng Sci.* 2000;456:1685–1709.
60. Yasui K, Tuziuti T, Iida Y, Mitome H. Theoretical study of the ambient-pressure dependence of sonochemical reactions. *J Chem Phys.* 2003;119:346–356.
61. Yasui K, Tuziuti T, Lee J, Kozuka T, Towata A, Iida Y. The range of ambient radius for an active bubble in sonoluminescence and sonochemical reactions. *J Chem Phys.* 2008;128:184705-1–184705-12.
62. Gong C, Hart DP. Ultrasound induced cavitation and sonochemical yields. *J Acoust Soc Am.* 1998;104:2675–2682.
63. Didenko YT, Pugach SP. Spectra of water sonoluminescence. *J Phys Chem.* 1994;98:9742–9749.
64. Buxton G, Greenstock C, Helman W, Ross A. Critical review of rate constants for reactions of hydrated electrons, hydrogen atoms and hydroxyl radicals (·OH/·O) in aqueous solution. *J Phys Chem Ref Data.* 1988;17:513–886.
65. Goldstein S, Czapski G. The reaction of no· with $O_2^-\cdot$ and $HO_2^-\cdot$: a pulse radiolysis study. *Free Radic Biol Med.* 1995;19:505–510.
66. Iida Y, Ashokkumar M, Tuziuti T, Kozuka T, Yasui K, Towata A, Lee J. Bubble population phenomena in sonochemical reactor: I. Estimation of bubble size distribution and its number density with pulsed sonication—laser diffraction method. *Ultrason Sonochem.* 2010;17:473–479.
67. Iida Y, Ashokkumar M, Tuziuti T, Kozuka T, Yasui K, Towata A, Lee J. Bubble population phenomena in sonochemical reactor: II. Estimation of bubble size distribution and its number density by simple coalescence model calculation. *Ultrason Sonochem.* 2010;17:480–486.
68. Brotchie A, Statham T, Zhou M, Dharmarathne L, Grieser F, Ashokkumar M. Acoustic bubble sizes, coalescence, and sonochemical activity in aqueous electrolyte solutions saturated with different gases. *Langmuir.* 2010;26:12690–12695.
69. Calderbank P, Moo-Young M. The continuous phase heat and mass transfer properties of dispersions. *Chem Eng Sci.* 1995;50:3921–3934.
70. Dudley J. Mass transfer in bubble columns: a comparison of correlations. *Water Res.* 1995;29:1129–1138.
71. Adewuyi Y, Owusu S. Aqueous absorption and oxidation of nitric oxide with oxone for the treatment of tail gases: process feasibility, stoichiometry, reaction pathways, and absorption rate. *Ind Eng Chem Res.* 2003;42:4084–4100.
72. McNamara W, Didenko Y, Suslick K. Sonoluminescence temperatures during multi-bubble cavitation. *Nature.* 1999;401:772–775.
73. Yasui K, Tuziuti T, Iida Y. Optimum bubble temperature for the sonochemical production of oxidants. *Ultrasonics.* 2004;42:579–584.
74. Khan NE, Adewuyi YG. Absorption and oxidation of nitric oxide (no) by aqueous solutions of sodium persulfate in a bubble column reactor. *Ind Eng Chem Res.* 2010;49:8749–8760.
75. Adewuyi YG. Sonochemistry in environmental remediation. 1. Combinative and hybrid sonophotochemical oxidation processes for the treatment of pollutants in water. *Environ Sci Technol.* 2005;39: 3409–3420.

Manuscript received July 31, 2010, and revision received July 26, 2011.